Marine Chemistry 223 (2020) 103801

Contents lists available at ScienceDirect

Marine Chemistry

journal homepage: www.elsevier.com/locate/marchem

Assessment of pH dependent errors in spectrophotometric pH measurements of seawater

Yuichiro Takeshita*, Kenneth S. Johnson, Luke J. Coletti, Hans W. Jannasch, Peter M. Walz, Joseph K. Warren

Monterey Bay Aquarium Research Institute, 7700 Sandholdt Road, Moss Landing, CA 95039, United States of America

ARTICLE INFO

Keywords:
Seawater pH
ISFET
Spectrophotometry
Meta-cresol purple

ABSTRACT

A recent analysis of full water column hydrographic data revealed a pH-dependent discrepancy between spectrophotometrically measured pH using purified meta-cresol purple and pH calculated from dissolved inorganic carbon (DIC) and total alkalinity (TA). The discrepancy ($pH_{spec} - pH_{TA,DIC}$) is approximately −0.018 and 0.014 at pH 7.4 and 8.2, respectively. This discrepancy has a wide range of implications for marine inorganic carbon measurements, such as establishing robust calibration protocols for pH sensors operating on profiling floats. Here, we conducted a series of lab based experiments to assess the magnitude of pH-dependent errors for spectrophotometric pH measurements in seawater by directly comparing its performance to pH measured by an Ion Sensitive Field Effect Transistor (ISFET) pH sensor known to have Nernstian behavior. Natural seawater was titrated with high CO_2 seawater while simultaneously measuring pH using spectrophotometry and an ISFET sensor over a large range in pH (7–8.5) and temperature (5–30 °C). The two pH measurements were consistent to better than ± 0.003 (range) at all temperatures except at 5 and 10 °C and very low and high pH, where discrepancies were as large as ± 0.005. These results demonstrate that pH-dependent errors in spectrophotometric pH measurements can be rejected as the cause of the pH-dependent discrepancy between pH_{spec} and $pH_{TA,DIC}$. The cause of this discrepancy is thus likely due to our incomplete understanding of the marine inorganic carbon model that could include errors in thermodynamic constants, concentrations of major ions in seawater, systematic biases in measurements of TA or DIC, or contributions of organic compounds that are not accounted for in the definition of total alkalinity. This should be a research priority for the inorganic carbon community.

1. Introduction

The idea that there are four 'master variables' in the marine carbonate system (total alkalinity (TA), dissolved inorganic carbon (DIC), partial pressure of CO_2 (pCO_2), and pH), and the knowledge of any two can be used to calculate the others, is a fundamental pillar in marine chemistry and is taught in introductory courses classes worldwide (Millero, 2007). Understanding this system is crucial in studying CO_2 dynamics in the ocean (Frankignoulle, 1994; Caldeira and Wickett, 2003), and thus the oceanic carbon cycle (Sabine and Tanhua, 2010; Takahashi et al., 2014). However, a recent analysis of hydrographic data in the Southern Ocean revealed that there is a pH dependent discrepancy between directly measured pH using spectrophotometry with purified meta-cresol purple (pH_{spec}) and pH calculated from TA and DIC ($pH_{TA,DIC}$), with a slope of 0.034 (Williams et al., 2017). This discrepancy was also present when the analysis was extended to the GLODAPV2 data set (Lauvset et al., 2016) with a slope of 0.0404, indicating that this is a global phenomenon (Carter et al., 2018). The discrepancy, defined as $pH_{spec} - pH_{TA,DIC}$, was approximately −0.018 and 0.014 at pH 7.4 and 8.2, respectively. These comparisons were based on shipboard measurements made at 1 atm, and at 20 or 25 °C. On the other hand, pCO_2, TA, and DIC seem to be internally consistent based on hydrographic data (Patsavas et al., 2015), suggesting that this discrepancy is specific to pH measurements.

This discrepancy has large implications for applications that intend to use pH measurements to constrain the marine carbonate system. In particular, autonomous pH measurements are becoming more common due to advancements in sensing technology (Martz et al., 2003, 2010; Seidel et al., 2008; Rérolle et al., 2012; Bresnahan et al., 2014, 2016; Lai et al., 2018; Ma et al., 2019), and integration onto autonomous platforms such as profiling floats (Johnson et al., 2016, 2017) and gliders (Hemming et al., 2017; Saba et al., 2019) for global observational networks (Bushinsky et al., 2019b; Claustre et al., 2020). Such pH data can be used, for example, to estimate seawater pCO_2 (Williams

* Corresponding author.
E-mail address: yui@mbari.org (Y. Takeshita).

https://doi.org/10.1016/j.marchem.2020.103801
Received 19 January 2020; Received in revised form 27 March 2020
Available online 04 April 2020

et al., 2017) to quantify air-sea fluxes (Gray et al., 2018; Bushinsky et al., 2019a) or seasonal dynamics (Takeshita et al., 2018; Williams et al., 2018). However, the accuracy of the estimated pCO_2 and other carbonate parameters is dependent on how well we understand the internal consistency of the marine inorganic carbon system. Small systematic biases can lead to large errors in the calculated air-sea fluxes. For example, a 1.3 μatm systematic bias in pCO_2 leads to a 0.2 Pg C yr^{-1} bias in the global integrated air-sea CO_2 flux (Wanninkhof et al., 2013). In the Southern Ocean, profiling float pH are corrected based on stable, deep ocean pH values that are typically low, and this discrepancy can cause a 1.6%, or ~ 6.4 μatm pCO_2 bias at the surface depending on if they were calibrated using pH_{spec} or $pH_{TA,DIC}$ (Williams et al., 2017). This would lead to unacceptably large errors in air-sea fluxes, thus poses a significant challenge in interpreting pH sensor data from autonomous platforms.

It is not clear where this pH-dependent discrepancy originates. The calculation of pH from TA and DIC relies on an inorganic thermodynamic model of the marine carbonate system, which requires accurate knowledge of equilibrium constants (e.g., K_1 and K_2 of carbonic acid in seawater (Dickson and Millero, 1987; Lueker et al., 2000) and others) and major ion concentrations (e.g., total boron concentrations (Uppstrom, 1974; Lee et al., 2010)), although there is substantial variability in these reported values (Millero, 2007). Uncertainties or errors in any of the multitude of the thermodynamic constants, as well as measurement uncertainties for TA, DIC, and pH can contribute to this observed discrepancy. Fong and Dickson, 2019 propagated the likely maximum uncertainty in the thermodynamic constants and measurement accuracies, and concluded that even in a 'worst case scenario', the trend in the $pH_{spec} - pH_{TA,DIC}$ differences could not be solely attributed to errors in thermodynamics. Thus, they concluded that the existence of an unaccounted for acid-base species that contributes to the total alkalinity such as organic acids is likely.

An alternative source of this discrepancy is a pH-dependent error in pH_{spec}. pH_{spec} is calibrated using equimolar Tris (2-amino-2-hydroxymethyl-1,3-propanediol) buffer in artificial seawater. The pH of this buffer solution is ultimately traceable to the Harned cell, which consists of the standard hydrogen electrode and a Ag/AgCl reference electrode (DelValls and Dickson, 1998; Pratt, 2014; Müller et al., 2018). While this provides excellent accuracy at the pH of the buffer solution, it is difficult to assess the accuracy over a range of pH. Typically, this is achieved by altering the temperature of the solution. However, this approach does not thoroughly assess pH-dependent errors over large pH ranges at a given temperature like that observed in Carter et al., 2018. Alternatively, a solution with different ratios of Tris could be prepared (Pratt, 2014), although this is labor intensive and can only be performed with certainty in laboratories that have access to the Harned Cell. Furthermore, currently there are multiple formulations for calculating pH_{spec} from absorbance, contributing to the uncertainty of pH_{spec} (Liu et al., 2011; DeGrandpre et al., 2014; Douglas and Byrne, 2017; Loucaides et al., 2017; Müller and Rehder, 2018). However, many of these equations focus on extreme conditions such as low salinity water in estuaries or in hypersaline solutions due to brine rejection, and the agreement between the studies at nominal seawater salinity is quite good. For example, DeGrandpre et al., 2014 observed an offset in pH_{spec} relative to Liu et al., 2011 of about 0.005, with a pH-dependent discrepancy of ~0.004, which is an order of magnitude smaller than the discrepancy between pH_{spec} and $pH_{TA,DIC}$. Nonetheless, the accuracy of pH_{spec} over a large range of pH at a constant temperature has not been rigorously examined.

The Honeywell Ion Sensitive Field Effect Transistor (ISFET) pH sensor, originally developed for industrial applications (Sandifer and Voycheck, 1999), exhibits exceptional performance in seawater (Martz et al., 2010). Its precision and stability is sufficient to quantify thermodynamic constants, such as the pressure effects on the pK_a of Tris buffer in artificial seawater (Takeshita et al., 2017). In particular, 100% Nernstian response of the ISFET to hydrogen ion activity was demonstrated over a pH range of 2–12 by directly comparing its response to the platinum Standard Hydrogen Electrode in a universal buffer solution with ionic strength similar to seawater (Takeshita et al., 2014). Over a pH range of 7–8.5, the maximum discrepancy between the ISFET and Standard Hydrogen Electrode was < 0.00005 pH, which is negligible. In other words, the ISFET can accurately measure changes in hydrogen ion activity, especially within nominal seawater pH range. This makes the ISFET a powerful tool to independently assess pH-dependent errors of pH_{spec} in seawater.

Here, we present results from an experiment to assess pH-dependent errors in pH_{spec} by directly comparing pH_{ISFET} and pH_{spec}. Measurements were made in natural seawater over a large range in pH at temperatures 5–30 °C using three independent ISFET sensors. Excellent agreement between the two measurements was observed at all temperatures, demonstrating that any biases that may exist in the pH_{spec} measurements cannot account for the observed pH-dependent discrepancy between pH_{spec} and pH_{TADIC}. This suggests that the pH-dependent discrepancy likely results from uncertainties and/or unknowns in the inorganic carbon model of seawater.

2. Methods

Natural seawater was titrated with high-CO_2 seawater titrant while simultaneously measuring pH_{spec} and pH_{ISFET} in a 1-L jacketed borosilicate beaker using a custom system (Fig. 1). Seawater was obtained from the flow through seawater system at MBARI, and was filtered using a 0.45 μm filter into a 20 L carboy (Bockmon and Dickson, 2014). This solution was bubbled with N_2 for ~3 days to reduce CO_2 prior to the experiment. The titrant was created by slowly bubbling 100% CO_2 in a 1 L aliquot of the same filtered seawater for at least 1 h immediately prior to the experiment. This approach only alters DIC and keeps TA and salinity constant through the titration. TA was measured using a Metrohm 855 autotitrator, following standard protocols (Dickson et al., 2007). Salinity was measured once per carboy after bubbling was finished using a density meter (Mettler Toledo DM45). The experiments were conducted at 5–30 °C at 5 degree intervals. The temperature was controlled using a recirculating water bath to better than ± 0.02 °C during each experiment. Temperature was measured inside the beaker using a NIST-traceable thermometer with an accuracy of ± 0.01 °C (QTI DTU6028–002).

The pH_{ISFET} was measured using a Honeywell ISFET as the pH electrode, and a chloride Ion Selective Electrode (Cl-ISE) as the reference electrode directly exposed to seawater (Martz et al., 2010). The electrodes were packaged in house (Johnson et al., 2016), and three separate electrodes were utilized for this study (DSD161, DSD200, and DSD208); these electrodes are the same type as those deployed on profiling floats. All electrodes were conditioned in flowing seawater for at least 3 weeks prior to the experiment. Custom electronics that contain the ISFET driving circuitry and a 24-bit ADC (Bresnahan et al., 2014) were used to measure the voltage between the Cl-ISE reference electrode and ISFET source (V_{RS}) and diagnostic currents to ensure proper electrode function. 10 measurements were averaged for each V_{RS}. The experiment was repeated in triplicate at 20 and 25 °C and in duplicates at all other temperatures for DSD161. The experiment was repeated in triplicate at 20 °C and carried out once at all other temperatures for DSD 200 and 208; DSD 200 and 208 were operated simultaneously in the same beaker. The ISFET measures pH on the free scale, and these values were converted to the total scale using the equilibrium constant for bisulfate from Dickson, 1990.

The DSD responds to both hydrogen ion and chloride ion activity in solution, and V_{RS} can be described by the Nernst equation (Martz et al., 2010):

$$V_{RS} = k_T - RT\ln(10)/F\ \log(m_{H+}) - RT\ln(10)/F\ \log(m_{Cl^-}) - RT\ln(10)/F\ \log(\gamma_{\pm HCl}{}^2)$$

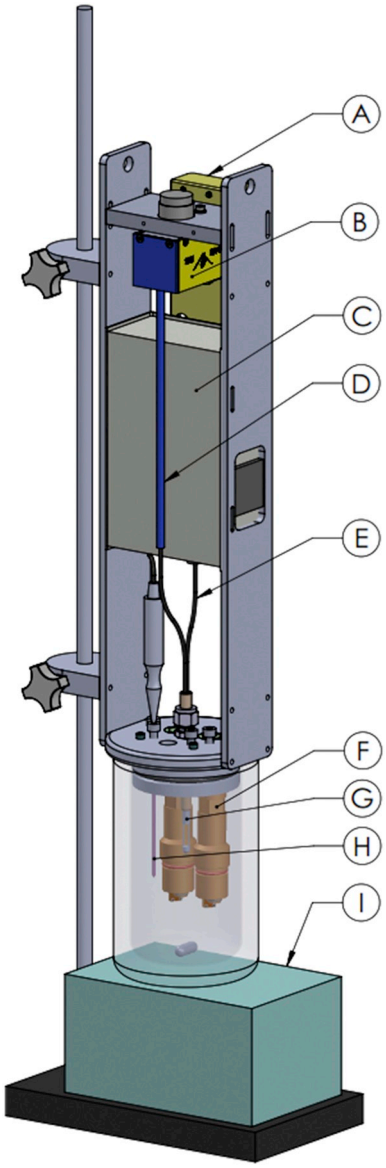

Fig. 1. Diagram of the experimental setup: (A) Controller operating DSD, spectrometer, and light source; (B) spectrometer; (C) light source; (D) fiber optical cable from solution to spectrometer; (E) fiber optical cable from light source to solution; (F) ISFET and Cl-ISE electrodes; (G) optical immersion probe; (H) thermometer; and (I) stir plate.

where R is the universal gas constant, F is the Faraday constant, T is temperature in Kelvin, m is the molality of the respective ions, and $\gamma_{\pm HCl}$ is the mean activity of HCl (Khoo et al., 1977). k_T is the temperature dependent calibration coefficient that is specific to each DSD, and is expressed by.

$$k_T = k_0 + k_2 \times T_C$$

where k_0 is the constant term, k_2 is the temperature coefficient, and T_C is temperature in Celsius. Measurements of V_{RS} at a constant temperature for given solution thus only reflects changes in m_{H+}, as all other terms remain constant. Small (~100 μV or ~ 0.0016 pH) variability in k_0 was observed between experiments where the electrode was removed from solution, rinsed with DI water, and briefly dried. Therefore k_0, or the constant term in the calibration coefficients for the DSD was determined for each experiment by averaging the k_0 obtained between pH of 7.8 and 7.85 using pH_{spec} as the reference pH. This range was chosen arbitrarily, since the results are not affected by which range of pH was used to determine k_0. It is emphasized that this small adjustment in k_0 manifests as a constant offset in pH_{ISFET}, and does not affect the ability for DSD to accurately measure changes in pH during each experiment.

The absorbance of the solution was measured directly inside the beaker using a custom 1-cm path length optical immersion probe (C-Technologies), optimized for low stray light and high transmission in the UV–Visible spectrum (200–780 nm) in seawater (Johnson and Coletti, 2002). A tungsten fiber optic light source (FO-6000; World Precision Instruments) and a fiber optic photo diode array spectrometer (MMS-UV/VIS; Zeiss 250–790 nm) was used for the light source and spectrometer, respectively. A custom interface board was used to communicate with the MMS-UV/VIS inside of a metal housing to minimize electrical and light interference. The spectrometer was further covered with black felt cloth to prevent any room light contamination. The light source was turned on only when making absorbance measurements (~5 s), as this led to better lamp stability over the experiment. When the lamp was left on, light intensity drifted significantly with a trend that seemed correlated with times when the cooling fan was actuated, indicating either a temperature or electrical effect. In general, light intensity at the non-absorbing wavelengths drifted by less than 200 counts out of ~45,000–50,000 (< 0.002 A) over 6 h. Dark currents were measured for each sample using the integrated shutter in the light source, and was typically around 1200 ± 15 (1 σ) counts. Stray light was determined by standard addition of m-cresol purple until the absorbance reached an asymptote, and was determined to be 80 counts (~0.2%) at 434 and 578 nm. pH_{spec} was calculated using constants presented in Liu et al., 2011.

At the beginning of each experiment, 800 mL of filtered seawater was added to the beaker, and sufficient time was allowed for the instrument measurements and temperature to stabilize, typically taking 1–2 h. The solution was stirred using a magnetic stir bar. Once stable, a blank spectrum was taken (n = 3), and 1.5 mL of 10 mM purified meta-cresol purple dye was added (Liu et al., 2011), which produced an absorbance at the isosbestic wavelength of ~0.15. Titrant was added at 200 μL increments using a MilliGAT LF gear pump. After each addition, the solution was mixed for 30 s, then triplicate measurements of absorbance and V_{RS} were made. A total of 200 additions were made per experiment, however, data were only interpreted when pH of the solution was within ± 1 of the pK_a of the indicator dye; the pK_a ranged from 7.94 to 8.31 in this temperature range. This resulted in approximately 100–120 titration points per experiment over 4–5 h. Obvious spikes in the data were removed (maximum 4, but typically none per experiment), which were presumed to be caused by bubbles in the optical pathway. The ΔpH (pH_{spec} − pH_{ISFET}) was calculated for each addition. The titration was automated through a custom LabView program.

In order to obtain accurate pH_{spec}, the wavelength accuracy and bandpass of the spectrometers used for the measurements and for deriving the constants must be comparable. To assess any potential errors in pH_{spec}, the performance of the pH_{spec} described above was assessed by directly comparing it to pH measured using the Agilent 8453 spectrometer ($pH_{spec,8453}$), which has a wavelength accuracy of 0.5 nm and bandpass of 3 nm, comparable to that used in Liu et al., 2011. Similar to the experiment above, natural seawater was titrated with CO_2, but the seawater solution was also recirculated into a temperature controlled 1-cm cell for the 8453 spectrometer using a Kloehn syringe pump. After each CO_2 addition, the solution was pumped into the 1-cm cell, 5 min were allowed for temperature to stabilize, and then absorbance was measured in triplicate. The experiment lasted < 1 h, and a total of 11 additions were conducted, ranging from seawater pH of 8.5 to 7.1.

3. Results

In general, excellent agreement was observed between pH_{spec} and pH_{ISFET}, and typical results from a single experiment are shown in

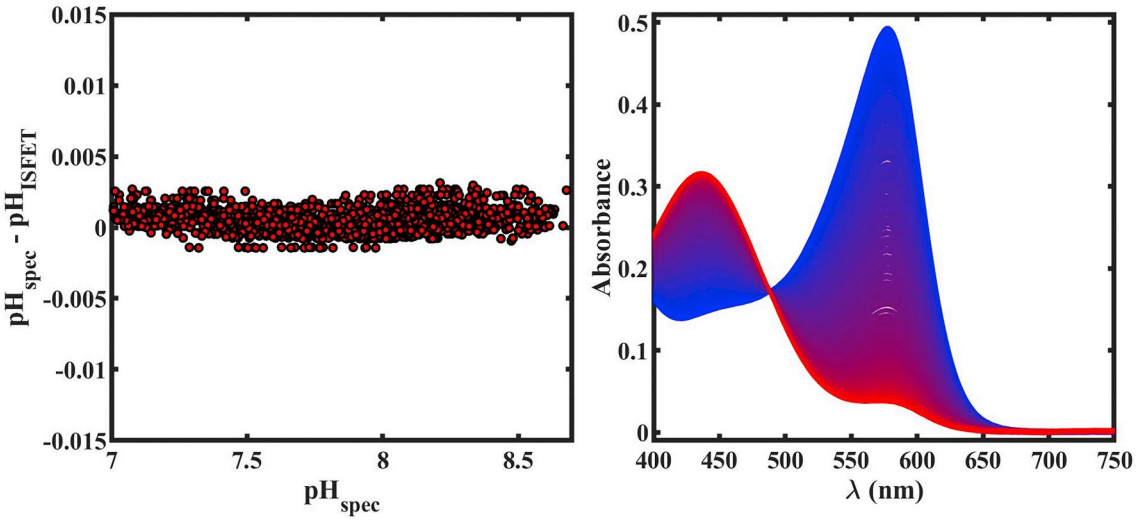

Fig. 2. Results from a typical experiment for ΔpH (pH_{spec} – pH_{ISFET}; left) and the compiled absorbance spectra (right).

Fig. 2. A decrease in the ratio of the absorbance at 578 and 434 nm are clearly seen as solution pH decreases throughout the titration. The isosbestic absorbance (~487 nm) does not change throughout the titration as it is not sensitive to pH, and only proportional to the concentration of indicator dye. Stability of the system is demonstrated in the non-absorbing wavelengths (> 730 nm), where absorbance was typically < 0.002 over several hours. A flat trend in ΔpH throughout the titration represents agreement between pH_{spec} and pH_{ISFET}, thus a lack of pH dependent errors in pH_{spec}. The average precision for pH_{spec} and pH_{ISFET} (1 σ, $n = 3$) after each CO_2 addition was ± 0.0008 and ± 0.0005, respectively. Salinity for DSD161 and DSD 200/208 was 33.7 and 33.86, respectively. TA was not measured for DSD161, but was 2226 ± 3 μmol kg^{-1} (1σ; $n = 12$) for DSD 200/208.

The results from all experiments are summarized in Fig. 3. Measurements from all experiments were binned to 0.02 pH intervals to calculate the mean and the 95% confidence interval (CI), shown in the black shaded error bar. The red dashed line in each plot represents the pH-dependent discrepancy observed in Carter et al., 2018 (−0.3168 + 0.0404pH), and the horizontal dashed lines represents ± 0.003 pH. In general ΔpH was did not vary as a function of pH, and remained below ± 0.003, although slightly larger variability and magnitudes of ΔpH was observed at lower temperatures (5–10 °C), especially at the high and low ends of pH, where spectrophotometric pH errors increase. Nevertheless, |ΔpH| was < 0.008 for all measurements. The averaged |ΔpH| was below 0.003, within the 95% CI except at 5 and 10 °C at very high and low pH, and always below 0.005 at all temperatures.

A constant negative bias, but no pH-dependent discrepancy was observed between the two spectrometers. On average, pH_{spec} was 0.0069 ± 0.0008 (1 σ) lower than $pH_{spec,8453}$ (Fig. 4). The variability in the residual is similar to that expected by propagating the precision of the pH measurements, which was ± 0.0007. The absorbance at 750–760 nm for the 8453 spectrometer was < 0.002 during this experiment, indicating minimal lamp drift.

4. Discussion

In all experiments, the ΔpH (pH_{spec} – pH_{ISFET}) was not sufficient to account for the pH-discrepancy between pH_{spec} and $pH_{TA,DIC}$ observed in GLODAPV2 (Carter et al., 2018). These experiments covered a large range in temperature (5–30 °C) and pH (7–8.5), and were conducted in natural seawater (Fig. 3). In fact, the magnitude of ΔpH over this large range in pH was below 0.003 (95% CI) at 20 and 25 °C, which are the temperatures that are commonly used for spectrophotometric pH aboard ships. There was no discernable trend over pH as well. This was true across all temperatures tested here, except at 5 and 10 °C, where ΔpH increased to ~0.005 at very low and high pH (Fig. 3). This demonstrates that no substantial pH-dependent error exists in pH_{spec}, and that the cause of the pH-dependent discrepancy is likely due to a combination of unknowns and biases in the marine inorganic carbon model. It was recently suggested that the observed pH-dependent discrepancy could only be explained by a combination of factors that included the presence of an additional acid/base species contributing to the total alkalinity that is not accounted for in the inorganic carbonate model (Fong and Dickson, 2019). The magnitude of this excess alkalinity is small, and is likely on the order of several μmol kg^{-1}, making it challenging to directly measure. Current methods to detect the excess alkalinity were developed for coastal applications, and are not sensitive enough for open-ocean applications (Yang et al., 2015). Development of sensitive techniques to directly measure the excess alkalinity is needed to test this hypothesis.

One of the strengths of this experiment is the fact that it was conducted in natural seawater. Alternatively, pH-dependent errors in pH_{spec} could have been assessed using artificial seawater solutions with different ratios of Tris buffer (Pratt, 2014). This approach has the benefit that the solutions could be directly traceable to the Harned Cell. However, it is significantly more labor intensive, and the presence of Tris alters the activity coefficients of the ionic media (DelValls and Dickson, 1998; Müller and Rehder, 2018), potentially creating biases relative to natural seawater. Conducting the experiments in natural seawater ensures that the results presented here are directly comparable to those from Carter et al., 2018.

In general, the |ΔpH| was less than 0.003, except sometimes at low temperatures or low pH. (Fig. 3) For example, ΔpH of −0.008 was observed for DSD161 at 5 °C, which was significantly larger in magnitude than the results from other temperatures or electrodes. However, it is important to note that there was at least one experimental run where |ΔpH| remained < 0.003 at all temperatures. The cause of the larger variability at lower temperatures is not clear. It is unlikely that drift in the light source is the primary cause, as the variability did not correlate with higher absorbance at 730 nm. One possibility is that small bubbles formed on the ISFET or the optical surface, leading to slight errors in the reading. The FET surface was visually inspected after every experiment, but no obvious bubbles were ever present. However, based on our experience, microbubbles that are not clearly visible can still cause problems for ISFET pH measurements. In addition, condensation that forms on the wires connecting the sensor and the electronics could potentially have caused small biases. Nonetheless, these are small errors

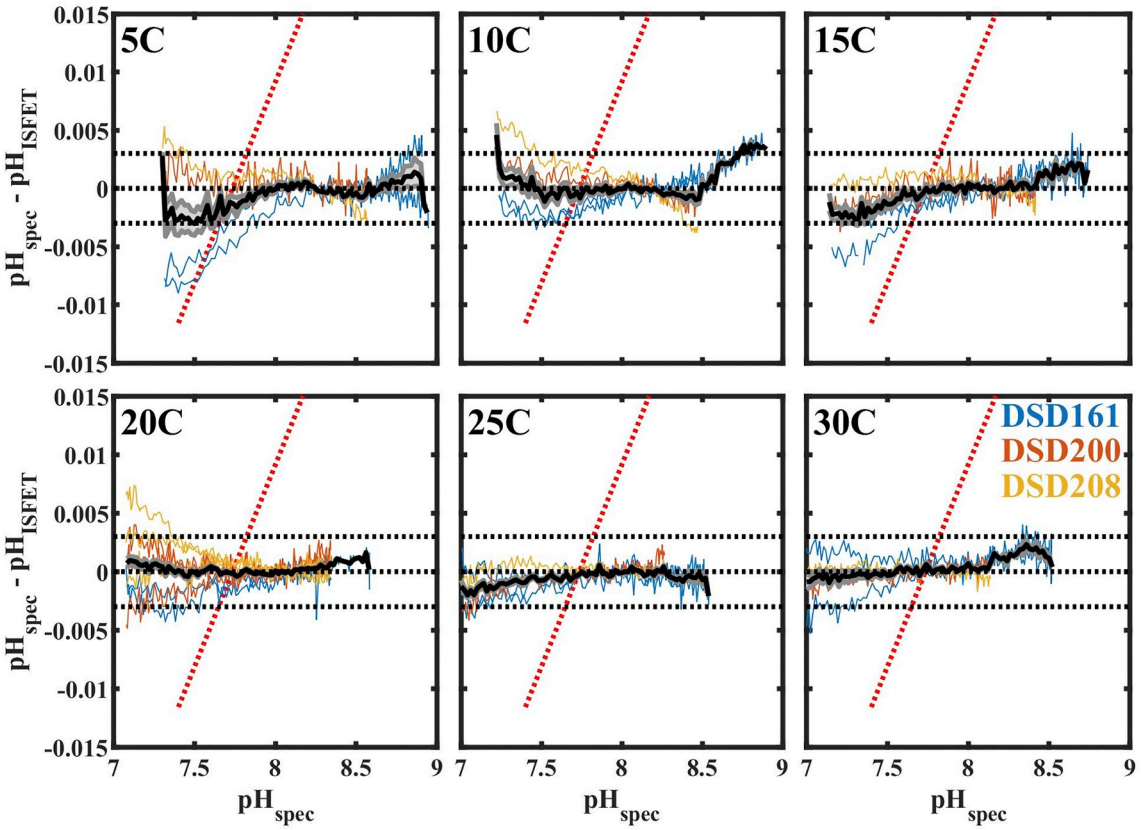

Fig. 3. Summary of experimental results. ΔpH (pH_{spec} - pH_{ISFET}) from DSD161 (blue), DSD200 (orange), and DSD208 (yellow) at each temperature, and the mean with the 95% CI is shown in black. Dashed black lines show ± 0.003, and the red dashed line is the observed pH dependent bias between pH_{spec} and $pH_{TA,DIC}$ from Carter et al., 2018. (For interpretation of the references to colour in this figure legend, the reader is referred to the web version of this article.)

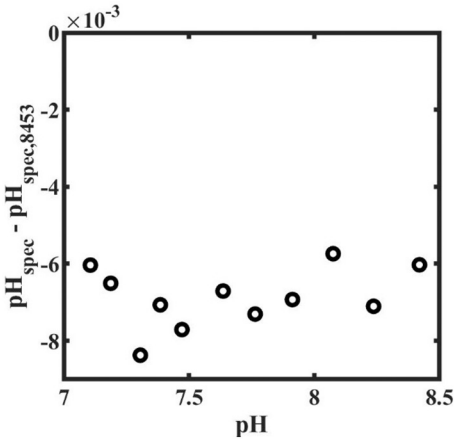

Fig. 4. Comparison between pH_{spec} measured using the FO-6000/MMS-UV/VIS (pH_{spec}) and the Agilent 8453 spectrometer ($pH_{spec,8453}$).

and do not affect the main conclusions of this manuscript.

Spectrophotometric pH measurements are subject to a variety of biases that include wavelength accuracy, spectral resolution, dye purity, and dye perturbation calculations (DeGrandpre et al., 2014), as well as other possible biases. The output wavelengths of the MMS-UV/VIS were verified using a Holmium oxide reference material, and is not a source of significant error here. In dispersive array spectrometers, the spectral resolution is a function of slit width, the diffraction grating, and the detector, and is ~7 nm (Δ λ Full Width Half Maximum FWHM) ≈ 7 nm) for the MMS-UV/VIS compared to ~3 nm (Δ λ FWHM ≈ 3 nm) for the Agilent 8453. A lower resolution (higher spectral bandwidth) means the spectrometer will integrate more "out of band" light, which leads to lower absorbance at a peak. Since the absorbance peak at 578 nm is sharper than at 434 nm, this leads to a lower absorbance ratio, thus lower pH (Fig. 4). The direct comparison between the two spectrometers demonstrates that while there is a negative offset as expected, no pH-dependent errors exist in the MMS-UV/VIS. Therefore, this spectrometer can be utilized for an accurate assessment for pH-dependent errors in pH_{spec}.

Another potential source of error could arise from different amounts of light-absorbing impurities remaining in the 'purified' indicator dye used in this study compared to that in Carter et al., 2018. Research groups that contributed to the GO-SHIP program obtained purified indicator dye from different sources (Personal comm. A. Dickson and R. Woosley), thus the potential for this bias cannot be ruled out. However, the predominant source of the purified meta-cresol purple for these cruises was USF, which is the same source used for this study. Each batch of dye from USF is specifically checked for impurities that absorb at 434 nm using HPLC (personal comm. X. Liu), which ensures consistent performance across dye batches. Therefore while this source of error is unlikely, it warrants further investigation. Finally, dye perturbation correction is not necessary for this experiment. This is because the objective is to compare pH_{spec} and pH_{ISFET} while they are simultaneously measuring the same solution. Since both pH measurements are made in a seawater solution with dye added to it, pH_{spec} should be reported for the solution pH after dye has been added, rather than the original pH of the solution prior to the addition of dye.

5. Conclusion

The main objective of this study was to determine whether there was a pH-dependent bias in the spectrophotometric pH method that could explain the pH-dependent discrepancy between pH_{spec} and

$pH_{TA,DIC}$ (Williams et al., 2017; Carter et al., 2018). Our results presented here demonstrate that pH-dependent errors in pH_{spec}, if any, are < 0.003 throughout the operating range for meta cresol purple, except potentially at low temperatures where they may be as large as ± 0.005. Thus, pH-dependent errors in pH_{spec} can be rejected as a significant cause of the observed discrepancy between pH_{spec} and $pH_{TA,DIC}$. Rather, it is likely a result of insufficient and incomplete characterization of the thermodynamic model of the marine inorganic carbon system. Determining the source of this bias should be a priority research topic, as it has worldwide implications for any laboratories making marine CO_2 chemistry measurements, as well as the calibration and application of autonomous pH sensor networks.

Acknowledgements

We thank the David and Lucile Packard Foundation for supporting this work.

References

Bockmon, E.E., Dickson, A.G., 2014. A seawater filtration method suitable for total dissolved inorganic carbon and pH analyses. Limnol. Oceanogr. Methods 12, 191–195. https://doi.org/10.4319/lom.2014.12.191.

Bresnahan, P.J., Martz, T.R., Takeshita, Y., Johnson, K.S., LaShomb, M., 2014. Best practices for autonomous measurement of seawater pH with the Honeywell Durafet. Methods Oceanogr. 9, 44–60.

Bresnahan, P.J., Wirth, T., Martz, T.R., et al., 2016. A sensor package for mapping pH and oxygen from mobile platforms. Methods Oceanogr. 17, 1–13. https://doi.org/10.1016/j.mio.2016.04.004.

Bushinsky, S.M., Landschützer, P., Rödenbeck, C., et al., 2019a. Reassessing Southern Ocean air-sea CO2 flux estimates with the addition of biogeochemical float observations. Global Biogeochem. Cycles 33, 1–19. https://doi.org/10.1029/2019GB006176.

Bushinsky, S.M., Takeshita, Y., Williams, N.L., 2019b. Observing changes in ocean carbonate chemistry: our autonomous future. Curr. Clim. Chang. Reports 5, 207–220. https://doi.org/10.1007/s40641-019-00129-8.

Caldeira, K., Wickett, M.E., 2003. Anthropogenic carbon and ocean pH. Nature 425, 365.

Carter, B.R., Feely, R.A., Williams, N.L., Dickson, A.G., Fong, M.B., Takeshita, Y., 2018. Updated methods for global locally interpolated estimation of alkalinity, pH, and nitrate. Limnol. Oceanogr. Methods 16, 119–131. https://doi.org/10.1002/lom3.10232.

Claustre, H., Johnson, K.S., Takeshita, Y., 2020. Observing the Global Ocean with biogeochemical-Argo. Annu. Rev. Mar. Sci. 12, 1–26. https://doi.org/10.1146/annurev-marine-010419-010956.

DeGrandpre, M.D., Spaulding, R.S., Newton, J.O., Jaqueth, E.J., Hamblock, S.E., Umansky, A.A., Harris, K.E., 2014. Considerations for the measurement of spectrophotometric pH for ocean acidification and other studies. Limnol. Oceanogr. Methods 12, 830–839. https://doi.org/10.4319/lom.2014.12.830.

DelValls, T.A., Dickson, A.G., 1998. The pH of buffers based on 2-amino-2-hydroxymethyl-1,3-propanediol ('tris') in synthetic sea water. Deep Sea Res. Part I Oceanogr. Res. Pap. 45, 1541–1554.

Dickson, A.G., 1990. Standard potential of the reaction : AgCl (s) + 1/2H2(g) = Ag (s) + HCl (aq), and the standard acidity constant of the ion HSO4- in synthetic sea water from 273. 15 to 318. 15 K. J. Chem. Thermodyn. 22, 113–127.

Dickson, A.G., Millero, F.J., 1987. A comparison of the equilibrium constants for the dissociation of carbonic acid in seawater media. Deep Sea Res. 34, 1733–1743.

Dickson, A.G., Sabine, C.L., Christian, J.R. (Eds.), 2007. Guide to best practices for ocean CO2 measurements. PICES Special Publication 3.

Douglas, N.K., Byrne, R.H., 2017. Spectrophotometric pH measurements from river to sea: calibration of mCP for 0 ≤ S ≤ 40 and 278.15 ≤ T ≤ 308.15 K. Mar. Chem. 197, 64–69. https://doi.org/10.1016/j.marchem.2017.10.001.

Fong, M.B., Dickson, A.G., 2019. Insights from GO-SHIP hydrography data into the thermodynamic consistency of CO 2 system measurements in seawater. Mar. Chem. 211, 52–63. https://doi.org/10.1016/j.marchem.2019.03.006.

Frankignoulle, M., 1994. A complete set of buffer factors for acid/base CO2 system in seawater. J. Mar. Syst. 5, 111–118.

Gray, A.R., Johnson, K.S., Bushinsky, S.M., et al., 2018. Autonomous biogeochemical floats detect significant carbon dioxide outgassing in the high-latitude Southern Ocean. Geophys. Res. Lett. 45, 9049–9057. https://doi.org/10.1029/2018GL078013.

Hemming, M.P., Kaiser, J., Heywood, K.J., et al., 2017. Measuring pH variability using an experimental sensor on an underwater glider. Ocean Sci. 13, 427–442. https://doi.org/10.5194/os-13-427-2017.

Johnson, K.S., Coletti, L.J., 2002. In situ ultraviolet spectrophotometry for high resolution and long-term monitoring of nitrate, bromide and bisulfide in the ocean. Deep Sea Res. Part I Oceanogr. Res. Pap. 49, 1291–1305. https://doi.org/10.1016/S0967-0637(02)00020-1.

Johnson, K.S., Jannasch, H.W., Coletti, L.J., Elrod, V.A., Martz, T.R., Takeshita, Y., Carlson, R.J., Connery, J.J., 2016. Deep-Sea DuraFET: a pressure tolerant pH sensor designed for global sensor networks. Anal. Chem. Acs. Analchem. 5b04653. https://doi.org/10.1021/acs.analchem.5b04653.

Johnson, K.S., Plant, J.N., Coletti, L.J., et al., 2017. Biogeochemical sensor performance in the SOCCOM profiling float array. J. Geophys. Res. Ocean. 122, 6416–6436. https://doi.org/10.1002/2017JC012838.

Khoo, K.H., Ramette, R.W., Culberson, C.H., Bates, R.G., 1977. Determination of hydrogen ion concentrations in seawater from 5 to 40.degree.C: standard potentials at salinities from 20 to 45%. Anal. Chem. 49, 29–34. https://doi.org/10.1021/ac50009a016.

Lai, C., DeGrandpre, M.D., Darlington, R.C., 2018. Autonomous optofluidic chemical analyzers for marine applications: insights from the submersible autonomous moored instruments (SAMI) for pH and pCO2. Front. Mar. Sci. 4, 1–11. https://doi.org/10.3389/fmars.2017.00438.

Lauvset, S.K., Key, R.M., Olsen, A., et al., 2016. A new global interior ocean mapped climatology: the 1° × 1° GLODAP version 2. Earth Syst. Sci. Data 8, 325–340. https://doi.org/10.5194/essd-8-325-2016.

Lee, K., Kim, T.W., Byrne, R.H., Millero, F.J., Feely, R.A., Liu, Y.M., 2010. The universal ratio of boron to chlorinity for the North Pacific and North Atlantic oceans. Geochim. Cosmochim. Acta 74, 1801–1811. https://doi.org/10.1016/j.gca.2009.12.027.

Liu, X., Patsavas, M.C., Byrne, R.H., 2011. Purification and characterization of meta-cresol purple for spectrophotometric seawater pH measurements. Environ. Sci. Technol. 45, 4862–4868. https://doi.org/10.1021/es200665d.

Loucaides, S., Rèrolle, V.M.C., Papadimitriou, S., Kennedy, H., Mowlem, M.C., Dickson, A.G., Gledhill, M., Achterberg, E.P., 2017. Characterization of meta-Cresol Purple for spectrophotometric pH measurements in saline and hypersaline media at sub-zero temperatures. Sci. Rep. 7, 1–11. https://doi.org/10.1038/s41598-017-02624-0.

Lueker, T.J., Dickson, A.G., Keeling, C.D., 2000. Ocean pCO2 calculated from dissolved inorganic carbon, alkalinity, and equations for K1 and K2: validation based on laboratory measurements of CO2 in gas and seawater at equilibrium. Mar. Chem. 70, 105–119. https://doi.org/10.1016/S0304-4203(00)00022-0.

Ma, J., Shu, H., Yang, B., Byrne, R.H., Yuan, D., 2019. Spectrophotometric determination of pH and carbonate ion concentrations in seawater: choices, constraints and consequences. Anal. Chim. Acta 1081, 18–31. https://doi.org/10.1016/j.aca.2019.06.024.

Martz, T.R., Carr, J.J., French, C.R., DeGrandpre, M.D., 2003. A submersible autonomous sensor for spectrophotometric pH measurements of natural waters. Anal. Chem. 75, 1844–1850.

Martz, T.R., Connery, J.G., Johnson, K.S., 2010. Testing the Honeywell Durafet for seawater pH applications. Limnol. Oceanogr. Methods 8, 172–184. https://doi.org/10.4319/lom.2010.8.172.

Millero, F.J., 2007. The marine inorganic carbon cycle. Chem. Rev. 107, 308–341. https://doi.org/10.1021/cr0503557.

Müller, J.D., Rehder, G., 2018. Metrology of pH measurements in brackish waters—part 2: experimental characterization of purified meta-cresol purple for spectrophotometric pHT measurements. Front. Mar. Sci. 5, 1–9. https://doi.org/10.3389/fmars.2018.00177.

Müller, J.D., Bastkowski, F., Sander, B., Seitz, S., Turner, D.R., Dickson, A.G., Rehder, G., 2018. Metrology for pH measurements in brackish waters—part 1: extending electrochemical pHT measurements of TRIS buffers to salinities 5–20. Front. Mar. Sci. 5, 1–12. https://doi.org/10.3389/fmars.2018.00176.

Patsavas, M.C., Byrne, R.H., Wanninkhof, R., Feely, R.A., Cai, W.J., 2015. Internal consistency of marine carbonate system measurements and assessments of aragonite saturation state: insights from two U.S. coastal cruises. Mar. Chem. 176, 9–20. https://doi.org/10.1016/j.marchem.2015.06.022.

Pratt, K.W., 2014. Measurement of pHT values of Tris buffers in artificial seawater at varying mole ratios of Tris: Tris·HCl. Mar. Chem. 162, 89–95. https://doi.org/10.1016/j.marchem.2014.03.003.

Rérolle, V.M.C., Floquet, C.F.A., Mowlem, M.C., Connelly, D.P., Achterberg, E.P., Bellerby, R.R.G.J., 2012. Seawater-pH measurements for ocean-acidification observations. TrAC Trends Anal. Chem. 40, 146–157. https://doi.org/10.1016/j.trac.2012.07.016.

Saba, G.K., Wright-Fairbanks, E., Chen, B., et al., 2019. The development and validation of a profiling glider deep ISFET-based pH sensor for high resolution observations of coastal and ocean acidification. Front. Mar. Sci. 6, 1–17. https://doi.org/10.3389/fmars.2019.00664.

Sabine, C.L., Tanhua, T., 2010. Estimation of anthropogenic CO2 inventories in the ocean. Annu. Rev. Mar. Sci. 2, 175–198. https://doi.org/10.1146/annurev-marine-120308-080947.

Sandifer, J.R., Voycheck, J.J., 1999. A Review of Biosensor and Industrial Applications of pH-ISFETs and an Evaluation of Honeywell's "DuraFET". Microchim. Acta 131, 91–98. https://doi.org/10.1007/s006040050013.

Seidel, M.P., DeGrandpre, M.D., Dickson, A.G., 2008. A sensor for in situ indicator-based measurements of seawater pH. Mar. Chem. 109, 18–28. https://doi.org/10.1016/j.marchem.2007.11.013.

Takahashi, T., Sutherland, S.C., Chipman, D.W., Goddard, J.G., Ho, C., 2014. Climatological distributions of pH, pCO2, total CO2, alkalinity, and CaCO3 saturation in the global surface ocean, and temporal changes at selected locations. Mar. Chem. 164, 95–125. https://doi.org/10.1016/j.marchem.2014.06.004.

Takeshita, Y., Martz, T.R., Johnson, K.S., Dickson, A.G., 2014. Characterization of an ion sensitive field effect transistor and chloride ion selective electrodes for pH measurements in seawater. Anal. Chem. 86, 11189–11195. https://doi.org/10.1021/ac502631z.

Takeshita, Y., Martz, T.R., Coletti, L.J., Dickson, A.G., Jannasch, H.W., Johnson, K.S., 2017. The effects of pressure on pH of Tris buffer in synthetic seawater. Mar. Chem. 188, 1–5. https://doi.org/10.1016/j.marchem.2016.11.002.

Takeshita, Y., Johnson, K.S., Martz, T.R., Plant, J.N., Sarmiento, J., 2018. Assessment of autonomous pH measurements for determining surface seawater partial pressure of CO 2. J. Geophys. Res. Ocean. 2–36. https://doi.org/10.1029/2017JC013387.

Uppstrom, L.R., 1974. The boron/chlorinity ratio of deep-sea water from the Pacific Ocean. Deep. Res. Oceanogr. Abstr. 21, 161–162. https://doi.org/10.1016/0011-7471(74)90074-6.

Wanninkhof, R., Park, G.H., Takahashi, T., et al., 2013. Global ocean carbon uptake: magnitude, variability and trends. Biogeosciences 10, 1983–2000. https://doi.org/10.5194/bg-10-1983-2013.

Williams, N.L., Juranek, L.W., Feely, R.A., et al., 2017. Calculating surface ocean pCO 2 from biogeochemical Argo floats equipped with pH: an uncertainty analysis. Global Biogeochem. Cycles 31, 591–604. https://doi.org/10.1002/2016GB005541.

Williams, N.L., Juranek, L.W., Feely, R.A., Russell, J.L., Johnson, K.S., Hales, B., 2018. Assessment of the carbonate chemistry seasonal cycles in the Southern Ocean from persistent observational platforms. J. Geophys. Res. Ocean. 1–20. https://doi.org/10.1029/2017JC012917.

Yang, B., Byrne, R.H., Lindemuth, M., 2015. Contributions of organic alkalinity to total alkalinity in coastal waters : a spectrophotometric approach. Mar. Chem. 176, 199–207. https://doi.org/10.1016/j.marchem.2015.09.008.